Role of Nek2 on centrosome duplication and aneuploidy in breast cancer cells

UNIVERSITÀ DEGLI STUDI DI TORINO

Role of Nek2 on centrosome duplication and aneuploidy in breast cancer cells

Paola Cappello[1,2*], Heiko Blaser[1*], Chiara Gorrini[1], Dan Chi Chia Lin[4], Andrew J. Elia[1], Andrew Wakeham[1], Syed Haider[3], Paul Botrous[3], Jacqueline M. Mason[4], Naomi A. Miller[5,6], Bruce Youngson[5,6], Susan Done[1,5,6] and Tak W. Mak[1+]

[1]The Campbell Family Institute for Breast Cancer Research, University Health Network, 620 University Avenue, Toronto, Ontario M5G 2M9, Canada

[2]Department of Molecular Biotechnology and Health Sciences, University of Turin, Turin, 10125-Italy

[3]Informatics & Biocomputing Platform, Ontario Institute for Cancer Research, Toronto, Ontario, M5G 0A3, Canada

[4]The Campbell Family Institute for Breast Cancer Research, University Health Network, TMDT East Tower, MaRS Centre, 101 College Street, 5-706, Toronto, ON, M5G 1L7, Canada.

[5]Laboratory Medicine Program, University Health Network, Toronto, ON, Canada

[6]Department of Laboratory Medicine and Pathobiology, University of Toronto, Toronto, ON, Canada

*PC and HB contributed equally to this work.

[+]Correspondence: Tak W. Mak, Ph.D.

Director, Campbell Family Institute for Breast Cancer Research

620 University Avenue, suite 706

Toronto, Ontario M5G 2M9, Canada

Tel: +1 416-946-2997 Fax: +1 416-204-5300

Email: tmak@uhnresearch.ca

Running head: Nek2 prevents aneuploidy in breast cancer cells.

Abstract

Breast cancer is the most common solid tumor and the second most common cause of death in women. Despite a large body of literature and progress in breast cancer research, many molecular aspects of this complex disease are still poorly understood, hindering the design of specific and effective therapeutic strategies. To identify molecules important in breast cancer progression and metastasis, we tested the *in vivo* effects of inhibiting the functions of various kinases and genes involved in the regulation/modulation of the cytoskeleton by downregulating them in mouse PyMT mammary tumor cells and human breast cancer cell lines. These kinases and cytoskeletal regulators were selected based on their prognostic values for breast cancer patient survival. PyMT tumor cells in which a selected gene was stably knocked down were injected into the tail veins of mice and the formation of tumors in the lungs was monitored. One of several genes found to be important for tumor growth in lungs was Nek2, a cell cycle-related protein kinase. Furthermore, Nek2 was also important for tumor growth in the mammary fat pad. In various human breast cancer cell lines, Nek2 knockdown induced aneuploidy and cell cycle arrest that led to cell death. Significantly, the breast cancer cell line most sensitive to Nek2 depletion was of the triple negative breast cancer subtype. Our data indicate that Nek2 plays a pivotal role in breast cancer growth at primary and secondary sites, and thus may be an attractive and novel therapeutic target for this disease.

Keywords: kinase, aneuploidy, cell cycle, breast cancer, cell death, metastasis

Introduction

Breast cancer is the most common female malignancy in North America and the second most common cause of cancer death in women (1). Breast tumors are classified into specific subtypes based on cellular morphology and the presence/absence of the estrogen receptor (ER), progesterone receptor (PR), and human epidermal growth factor receptor-2 (ERBB2/HER2). Examinations of each subtype's pathophysiology have generated targeted therapies that have extended the survival of some patients with metastatic breast cancers. Such therapies, which include taxanes, aromatase inhibitors, and trastuzumab (2, 3), have significantly improved outcomes for patients with breast cancers of the luminal or HER2 subtypes. Sadly, an effective targeted treatment is still lacking for patients whose tumors are of the highly aggressive triple negative breast cancer (TNBC) subtype (4, 5).

Because kinases are crucial for cancer cell survival, mitosis, migration and invasion, much research has been focused on developing inhibitors against them (6-8). Rapidly proliferating tumors like TNBCs rely on tight temporal regulation of the cell cycle and centrosome duplication. Inhibition of kinases associated with mitosis induces severe defects in centrosome duplication and chromosome segregation that ultimately lead to aneuploidy and cell death (9-12). The future of TNBC management may therefore lie in the identification of new cell cycle regulators that control breast cancer progression and metastasis.

The Nek proteins belong to a family of serine/threonine kinases named after the NIMA gene originally cloned in *Aspergillus nidulans* (14). In mammals, there are 11 family members (Nek1-Nek11) but only four of these proteins, Nek2, Nek6, Nek7 and Nek9, play roles in mitotic progression (15). Of particular interest is Nek2, which localizes to the centrosome/centriole and

helps to establish a bipolar spindle by initiating the separation of centrosomes (16-18). High levels of NEK2 protein have been previously described in breast cancers (19), and Nek2 mRNA overexpression has been reported in different breast cancer subtypes (20, 21). These observations, coupled with Nek2's function as a major centrosome regulator, marks this kinase as an emerging target of drug discovery interest (43-45).

In this study, we show that cancer cells lacking Nek2 exhibit aberrant mitosis leading to apoptosis. Furthermore, Nek2 knockdown in cancer cells induces aneuploidy, cell cycle arrest, and caspase-dependent and -independent cell death. Mechanistically, Nek2 depletion promotes the activity of the tumor suppressor pRb while simultaneously reducing the activation of the cell division regulator histone H3. *In vivo*, mouse and human cancer cells lacking Nek2 expression grow more slowly than control cells and give rise to reduced tumor burden in the lungs. Our results suggest that Nek2 inhibition could help to disrupt the cell cycle of TNBC cells, enhancing the effects of current chemotherapeutic interventions.

Results

High Nek2 expression correlates with poor prognosis in breast cancer patients

To identify specific kinases and cytoskeletal regulators important for breast cancer cell survival *in vivo*, we used stable expression of short-hairpin RNA (shRNA) to silence genes encoding selected cytoskeletal regulators and kinases in mouse PyMT mammary tumors [PyMT cells, previously described in (13)]. We selected candidates whose high expression correlated positively with greater risk of patient mortality as evaluated in a cohort of 2312 breast cancer patients (Figure 1a). By choosing a cut-off of 1.2 for the hazard ratio (HR), we compiled a list of 14 target genes suitable for further study *in vivo*. We silenced each gene individually in PyMT cells (Supplementary Figure S1a) and intravenously (IV) injected the modified cells into syngeneic recipient mice. The recipients have been monitored to assess if the lack of each target gene is able to suppress tumor growth in the lung (Supplementary Figure S1b). Based on our *in vivo* results and the pharmacological tractability of our 14 genes (as determined by consulting sources such as ChEmbl, PubChem, Drugbank and Sophic Druggable Genome), we chose Nek2 for further in-depth investigation. We first confirmed that Nek2 mRNA is overexpressed in basal-like as well as non-basal-like breast cancers in comparison to normal breast tissue (Figure 1b), and showed that Nek2 overexpression correlates positively with a greater risk of patient mortality (Figure 1c). We also demonstrated that Nek2 overexpression correlates positively with disease recurrence (Figure 1d) (22) in breast cancer patients. In order to correlate NEK2 protein expression between normal and malignant breast tissue we performed immunohistological analysis on a tissue microarray (TMA) comprised of TNBC samples from a cohort of 39 patients (Supplementary Table S1). Invasive ductal carcinomas (IDCs) showed a markedly increased

number of cells expressing nuclear NEK2 in comparison to normal breast tissue (Figure 1e, f). Notably, about 45% of all normal breast tissue showed zero nuclear NEK2 expression intensity whereas only about 5% of IDCs were considered to have no expression. Conversely, about 36% of all IDCs showed strong nuclear NEK2 expression in comparison to about 3% of normal breast tissue samples (Figure 1g). These results affirm the relevance of evaluating Nek2 as a potential target in human breast cancer.

Nek2 promotes the growth of PyMT cells in the lung

To study the role of Nek2 in tumor growth, we stably knocked down Nek2 in luciferase-expressing PyMT cells using specific shRNA (PyMT-shNek2) (Figure 2a, b). We then injected PyMT-shNek2 or PyMT-ctr cells (expressing scramble shRNA) into female syngeneic mice via the tail vein and performed live animal imaging to monitor tumor growth in the lungs. At 4 weeks post-injection, tumor cell engraftment was readily detected in all mice injected with PyMT-ctr cells but rarely in mice injected with PyMT-shNek2 cells (Figure 2c). Moreover, while all control mice died by 20 weeks post-injection, 50% of mice injected with PyMT-shNek2 cells survived past that timepoint, and 20% of these mice were still alive at 50 weeks post-injection (Figure 2d).

Because of Nek2's known role in mitotic progression (18), we analyzed the cell cycle in PyMT-shNek2 and control cells after serum starvation or nocodazole treatment. Nek2 knockdown increased the G1 population and modestly enhanced the G2/M population, indicating that cell cycle arrest had occurred (Figure 2e, f). However, the most interesting effect of Nek2 silencing was the eventual generation of an aneuploid cell population. This aneuploid subset comprised 64% of all PyMT-shNek2 cells at 48 hrs after serum replenishment but was virtually

absent (0.3% at 48 hrs) in control cells (Figure 2e, g). A similar trend was observed following release from nocodazole treatment (Supplementary Figure S2). We hypothesized that this induction of aneuploidy upon Nek2 knockdown could underlie the observed increase in G1 cells, and might explain the significant reduction in tumor growth in mice bearing PyMT-shNek2 cells.

Nek2 promotes the growth of human breast cancer cells in vivo

To determine whether Nek2 is also important for the cell cycle in human breast cancer cells, we transduced luciferase-expressing MDA-MB-231 cells (TNBC cell line) with either scramble shRNA (MDA-MB-231-ctr) or Nek2 shRNA (MDA-MB-231-shNek2) (Figure 3a, b). A previous study showed that the *in vivo* growth of MCF7 or MDA-MB-231 human breast cancer cells could be inhibited by injecting siRNA against Nek2 directly into tumors (23). We injected MDA-MB-231-shNek2 or control cells into either the tail veins of NOD-SCID mice, or into the fat pads of female NIH-III mice. In NOD-SCID mice, even at 3 weeks post-injection, we detected more tumor cells in the lungs of the animals injected with control cells than in the lungs of those injected with MDA-MB-231-shNek2 cells (Figure 3c). While all control NOD-SCID mice died by 6 weeks post-injection, 20% of NOD-SCID mice injected with MDA-MB-231-shNek2 cells were still alive at 10 weeks post-injection (Figure 3d). Similarly, MDA-MB-231-shNek2 cells injected into the fat pads of NIH-III mice generated tumors that were significantly smaller than those derived from control cells (Figure 3e). Histological analysis of lungs excised from NOD-SCID mice at 5 weeks post-injection confirmed the presence of a significantly reduced tumor burden in animals that received MDA-MB-231-shNek2 cells compared to those injected with control cells, as indicated by the reduced ratio of tumor area to normal tissue in the

former group (Figure 3f). These findings suggest that Nek2 promotes the growth of human breast cancer cells in primary and secondary sites.

Nek2 depletion results in cell cycle defects, centrosomal alterations, and aneuploidy in human breast cancer cells

To understand Nek2's pro-tumorigenic role in human breast cancer cells, we evaluated the cell cycle progression of MDA-MB-231-shNek2 cells. We detected a large aneuploid cell population that represented 20-30% of all serum-starved cells, and 60-80% of all nocodazole-treated cells (Figure 4a, c and Supplementary Figure S3). Compared to cultures of PyMT-shNek2 cells, MDA-MB-231-shNek2 cells showed a larger increase in the subG1 population (dead cells; Figure 4b). Furthermore, the proliferative capacity of MDA-MB-231-shNek2 cells was reduced compared to control cells (Figure 4d), a defect confirmed by the decreased percentage of $BrdU^+$ cells detected in MDA-MB-231-shNek2 cultures (Figure 4e, f). This impaired proliferation in the absence of Nek2 was also observed in several other human breast cancer cell lines subjected to Nek2 knockdown, including HCC1806 cells (TNBC), T47D cells (luminal A breast cancer), and MCF7 cells (luminal A breast cancer) (Supplementary Figure S4). Interestingly, the responses of different human breast cancer cells to Nek2 knockdown were not uniform. HCC1806-shNek2 cultures showed an abnormally high percentage of cells in the G2/M and subG1 phases but no aneuploidy (Supplementary Figure S5). In contrast, both an aneuploid cell population and an expanded subG1 population were detected in T47D-shNek2 cells (Supplementary Figure S6). MCF7-shNek2 cells displayed a decreased proliferation rate compared to controls, in line with their slight increase in G2/M phase (Supplementary Figure S7). These results emphasize the heterogeneity of human breast cancers but also suggest that inhibition of Nek2 can interfere with

the growth of different breast cancer subtypes. The reduced tumor burden observed in the lungs of mice injected with MDA-MB-231-shNek2 cells (refer to Figure 3f) could also result from defects in cell migration or invasion. We therefore evaluated these capacities in MDA-MB-231-shNek2 cells using real-time and transwell migration and invasion assays. MDA-MB-231-shNek2 cells showed slightly decreased migration ability compared to control cells but no difference in invasion capacity (Supplementary Figure S8). These data imply that the reduced growth of Nek2-depleted cells in lungs is mainly due to cell cycle abnormalities, aneuploidy, and cell death, with little or no contribution by a defect in either migration or invasion.

To confirm the appearance of aberrant multicentrosomal and multinuclear cells in MDA-MB-231-shNek2 cultures, we stained the cells with antibodies recognizing α-tubulin, pericentrin or centrin2 to visualize microtubules, centrosomes and centrioles, respectively. While most control cells displayed two centrosomes and normal mitotic spindles, many MDA-MB-231-shNek2 cells showed multiple centrosomes and aberrant mitotic spindles (Figure 5a). An increase in centrosome numbers in the absence of Nek2 was confirmed by the quantitation of the number of centrioles per pole (Figure 5b). We then evaluated the percentage of cells undergoing monopolar, bipolar or multipolar division in control and MDA-MB-231-shNek2 cultures. Nek2 knockdown cultures showed a significantly lower percentage of cells with bipolar division, and consequently a higher percentage of cells with multipolar division compared to controls (Figure 5c). Furthermore, karyotype analysis confirmed a markedly greater number of chromosomes per cell in MDA-MB-231-shNek2 cultures compared to controls (Figure 5d, e).

To determine the fate of cells lacking Nek2, we used real-time microscopy and MDA-MB-231 cells engineered to both (1) co-express doxycycline (DOX)-induced shNek2 and red fluorescent protein (RFP), and (2) express GFP-conjugated histone 2B (H2B-GFP; to label chromosomes).

In the absence of DOX (wild type Nek2 expression), the majority of H2B-GFP-expressing MDA-MB-231 cells divided normally into two daughter cells (Figure 5f and Supplementary Movie 1). However, when Nek2 knockdown was induced by DOX, the cells exhibited aberrant mitosis. Multinuclear cells in these cultures ultimately suffered a mitotic catastrophe and underwent apoptosis-like death characterized by extensive membrane blebbing (Figure 5f and Supplementary Movie 2). Thus, Nek2 knockdown disrupts the centrosomal machinery, inducing aberrant mitosis that produces aneuploid and multinuclear cells and ultimately leads to cell death.

Nek2 knockdown increases caspase-3 cleavage and alters pRb and histone H3 activity

To verify if the enhanced subG1 population in MDA-MB-231-shNek2 cultures reflected an increase in apoptotic cells, we used flow cytometry to evaluate the percentage of cells positive for cleaved caspase-3 (CC-3^+). After 48 hrs, the percentage of CC-3^+ cells in control cultures was about 4%, whereas MDA-MB-231-shNek2 cultures displayed 4 times more CC-3^+ cells (Figure 6a, left). The addition of zVAD, a pan-caspase inhibitor, did not change the percentage of CC-3^+ cells in control cultures but significantly decreased the percentage of CC-3^+ cells in MDA-MB-231-shNek2 cultures (Figure 6a, left). Application of zVAD also decreased the subG1 population among MDA-MB-231-shNek2 cells by 20% but had no effect on the subG1 population in the control (Figure 6a, right). Increased apoptosis in the absence of Nek2 was also confirmed by immunohistochemical analysis of CC-3 in tumors isolated from xenografted NIH-III mice. More CC-3^+ cells were observed in tumors from animals xenografted with MDA-MB-231-shNek2 cells compared to tumors from control animals (Figure 6b). At the molecular level, MDA-MB-231-shNek2 cells revealed reduced phosphorylated pRb and phosphorylated histone H3-Ser10 compared to controls (Figure 6c). This result is in line with previous observations that

hypophosphorylated pRb functions as a tumor suppressor by inhibiting cell cycle progression, and that phosphorylated histone H3-Ser10 is required for normal chromosome segregation (24, 25). The fact that abnormalities in these vital cell cycle factors are observed when Nek2 is depleted further substantiates our contention that Nek2 is required for proper cell cycle progression and chromosome segregation.

Discussion

Over the past few decades, huge efforts have been undertaken to identify new key players in breast cancer progression and metastasis. It is well known that tumor cells act completely differently in culture than they do *in vivo*, where they are surrounded by stromal cells and interact with cells of the immune system. These considerations led us to use living animals to test a selection of putative therapeutic targets relevant to breast cancer. We have identified several kinases and cytoskeletal regulators that, when knocked down, reduce or completely inhibit tumor growth *in vivo*. The particular target examined in this study was Nek2, which is overexpressed in cases of all subtypes of breast cancer. Such overexpression is likely due to amplification of chromosomal region 1q32, which contains the human Nek2 locus (26). In our study, we have confirmed that Nek2 overexpression correlates positively with higher risks of disease recurrence and mortality in breast cancer patients. We have also shown that Nek2-depleted human breast cancer cells grow poorly in the lungs and mammary fat pads of xenografted mouse recipients. Others have previously reported that Nek2 has a pivotal role in tumor cell growth and apoptosis (23, 27), we propose that the main effects of Nek2 depletion are a block in cell cycle progression and interference with chromosomal segregation, leading to aneuploidy and subsequent cell death.

We observed that human breast cancer cells lacking Nek2 proliferated less than control cells and displayed a higher percentage of cells in the G2/M phase. Moreover, cultures of mouse PyMT cells and human TNBC cells both showed a huge population of aneuploid cells and a parallel increase in the subG1 population. Aneuploidy and chromosome instability are common abnormalities in human cancers and are linked to poor clinical outcome (32). Loss of control over mitotic progression, spindle formation, and cytokinesis are all likely to contribute to these abnormalities. However, aneuploidy and aberrant mitosis can also precipitate chromosomal

breakage or interchromosomal concatenation, resulting in a lethal genetic imbalance that leads to cell death. Thus, aneuploidy can be a promoter or suppressor for mutations that inhibit tumor cell growth or induce cell death (33). Our data show that Nek2 knockdown cells display multipolar centrosomes and aberrant mitotic figures. Nek2 is known to phosphorylate mitotic checkpoint proteins such as Mad2 and Cdc20 (34), and to interact with the spindle assembly checkpoint protein Mad1 (31). Nek2 also contributes to the microtubule reorganization necessary for the G2/M transition by phosphorylating several centrosomal substrates, including c-Nap1, rootletin, PP1, Nlp, centrobin and HMGA2 (28, 29). In accordance with these observations, we could demonstrate that multinuclear cells that lack Nek2 died during mitosis. We also found a higher percentage of CC-3$^+$ cells in tumors of mice injected with Nek2 knockdown cells compared to tumors of mice injected with control cells. Taken together, these data suggest that the aneuploidy associated with Nek2 depletion can induce cancer cell death.

Phosphorylation of histone H3-Ser10 is required for normal chromosome condensation and segregation. Our study has shown that Nek2 depletion greatly reduces histone H3-Ser10 phosphorylation. *In vitro*, Nek2 can phosphorylate histone H3 either directly or through Erk1/p90Rsk2, but it remains under debate if Nek2 can phosphorylate histone H3 *in vivo* (18, 35, 36). In addition, although a direct link between Nek2 and pRb regulation has yet to be reported, we have demonstrated that Nek2 depletion decreases the level of pRb phosphorylation. This reduction could allow more pRb molecules to remain active and inhibit cell cycle progression. Alternatively, Nek2 and pRb signaling could be interconnected through the mitotic kinetochore protein Hec1. Previous work has shown that Nek2 may participate in chromosome condensation through its interactions with Hec1 (30), and Nek2-dependent phosphorylaton of Hec1 is essential for kinetochore attachments to microtubules during mitosis (37). Hec1 is functionally linked to

the pRb pathway because disruption of pRb activity leads to Hec1 overexpression, inducing defects in chromosome segregation and mitosis (38). Collectively, these data suggest that Nek2 may be involved in regulating both the histone H3 and pRb pathways.

Interference with mitosis is a well-recognized modality of anti-cancer therapy. The chemotherapeutic drug Taxol triggers cell death by inactivating the spindle checkpoint, thus inducing aneuploidy and aberrant mitosis (39). Kinase inhibitors that have the same effects on tumor cells might therefore be helpful adjuncts when used in combination with chemotherapeutic drugs based on other strategies. Viridin analogs, which are highly specific inhibitors of Nek2, can induce centrosome disruption and inhibit cancer cell growth *in vitro* (40). Other recent work has indicated that Nek2 silencing can induce apoptosis of cells that show chromosomal instability but not of cells with a normal karyotype (41, 42). Our study provides *in vivo* validation of the concept that Nek2 is important for tumor growth in both primary and secondary sites, and strengthens the rationale underlying the growing efforts to develop specific therapeutic inhibitors against this kinase.

Material and Methods

Cell lines and plasmids

PyMT mammary tumor cells were derived from MMTV-PyMT mice and maintained as previously reported (13). All human breast cancer cell lines (MDA-MB-231, HCC1806, T47D, MCF7) were obtained from ATCC. Unless otherwise indicated, all cell lines were maintained in complete medium (CM), which was DMEM supplemented with 10% fetal bovine serum (FBS). For serum starvation, cells were cultured overnight in serum-free DMEM. For nocodazole treatment, cells were cultured overnight in CM containing 100 ng/ml nocodazole (Sigma). For stable knockdown, control scramble shRNA and gene-specific shRNAs were purchased for lentiviral expression: pLKO.1 for mouse PyMT cells, and pGIPZ/pTRIPZ for human breast cancer cells (Sigma, Open Biosystems).

Microarray analysis

i) Datasets used: We developed a database comprised of 15 publicly available mRNA expression datasets (PMIDs: 16273092, 17545524, 16141321, 16280042, 16478745, 18498629, 17157792, 19421193, 20098429, 20064235, 20490655, 20697068, 18821012, 18593943, 15721472). Raw data was pre-processed using the RMA algorithm (12582260) with Entrez Gene annotation (PMID: 16284200). Pre-processing was performed in the R statistical environment (v2.11.1) using the affy package of BioConductor (v1.26.1) and v12.1.0 of the updated Entrez Gene annotation packages.

ii) Ortholog mapping: Human genes were mapped to their mouse orthologs using the Homologene database (build 64) and custom perl scripts.

iii) Statistical analysis and data visualization: Signal intensities of each candidate gene were median-dichotomized in each dataset, as outlined previously (PMID: 20696928), in the R statistical environment (v2.12.1). Survival rates of patients in the "good" and "poor" outcome groups were compared using unadjusted Cox proportional hazards modeling, as implemented in the survival package (v2.36-5). Gene association with patient prognosis: the Wald test was employed to determine if the hazard ratio (HR) was statistically different from unity. Kaplan-Meier curves were created using the lattice (v0.19-19) and latticeExtra (v0.6-15) packages.

Quantitative real-time PCR

TRIzol reagent (Invitrogen) was used for total RNA extraction and the iScript reverse transcription kit (BioRad) was used to produce cDNA. qRT-PCR reactions were performed in triplicate using SYBR Green mix (AppliedBiosystems) and an Applied Biosystems Real-time PCR-7900HT instrument. The amplification of the *gapdh*/GAPDH gene was used as an internal reference control.

Cell proliferation

Cells were cultured for up to 6 days in CM. Cells were stained with trypan blue and analysed using a Vi-Cell XR instrument (Beckman Coulter) to determine viability and establish growth curves. For real-time cell proliferation, cells were subjected to serum starvation or nocodazole treatment as described above, cultured in CM for an additional 5 days, and monitored using an xCELLigence RTCA DP device (Roche Diagnostics). The proliferation rate was expressed as the slope [1/h], where a higher slope represents faster cell growth. Cell proliferation was also analysed by BrdU incorporation and flow cytometry. Briefly, serum-starved or nocodozole-

treated cells were cultured overnight in CM containing BrdU starting at 24 hrs or 72 hrs after CM replenishment. BrdU incorporation was detected using the APC-BrdU kit (BD) following the manufacturer's instructions.

Migration and invasion assays

Transwell filters coated with collagen-I or Matrigel (BD Biosciences, 8 μm pore size) were used for migration or invasion assays, respectively. Cells ($2.5x10^4$ for migration assays or $5x10^4$ for invasion assays) were seeded into the upper chamber in DMEM with 0.5% FBS. The bottom chamber contained DMEM with 20% FBS. Cells were allowed to migrate/invade at 37°C in 5% CO_2 for 20 hrs before they were fixed and stained in methanol/methylene-blue solution. Cell counts were performed on 10 fields per filter, and the mean was normalized to the migration/invasion cell count of control cells. Real-time cell migration was evaluated using the xCELLigence RTCA DP device (Roche Diagnostics). For this purpose, $1x10^4$, $2x10^4$ or $4x10^4$ MDA-MB-231 cells per well were seeded in CIM-Plates 16 (Roche Diagnostics). The migration rate was expressed as the slope [1/h], where a higher slope represents faster cell movement.

Cell cycle analysis

Cells ($2x10^5$) were cultured overnight in serum-free medium or in CM containing nocodazole (100 ng/ml). The medium was changed to CM and the cells were cultured for 24, 48, 72, 96 or 120 hrs. After ethanol fixation, cells were washed with PBS, suspended in PBS containing 2 μg/ml propidium iodide (Sigma) plus 20 mg/ml RNAse (Invitrogen), and examined using a FACSCalibur instrument and ModFit software (BD Biosciences). To evaluate CC-3^+ cells by flow cytometry, the PE Active Caspase-3 Apoptosis Kit (BD Biosciences) was used following

the manufacturer's instructions. Cells were acquired and analysed with CellQuest software (BD Biosciences). For caspase inhibitor studies, cells were cultured in CM containing 50 μM zVAD (Sigma) for 48 hrs prior to cell cycle analysis as described above. CC-3^+ cells without zVAD were evaluated in a parallel set of plates as a control.

In vivo analyses of tumor growth

Luciferase-expressing MDA-MB-231 or PyMT cells ($2.5x10^5$ in 200μl PBS) co-expressing scramble or gene-specific shRNAs were injected into the tail vein of 8-week-old NOD-SCID or 129P2Ola female recipients, respectively. Imaging of luciferase-expressing tumor cells was performed using the Xenogen system (IVIS, Caliper Life Sciences). Mouse survival was evaluated using Kaplan-Meier methodology. For *in vivo* tumor growth analysis, control MDA-MB-231 or MDA-MB-231-shNek2 cells were injected into the fat pads ($1x10^6$ cells in Matrigel) of 8-week-old NIH-III *nu/nu* mice, or into the tail vein ($2.5x10^5$ cells in 200μl PBS) of NOD-SCID female mice. After 35 days, recipient mice were sacrificed and tumors and lungs were excised. Tumor weights were recorded and tissues processed for further analysis. All animal experiments were approved by the Animal Care and Use Committee of the University Health Network (Toronto, Canada).

Karyotyping

Cells were cultured in CM containing nocodazole (100 ng/ml) for 5 hrs before treatment with hypotonic solution (0.56% KCl) and fixation in methanol/acetic acid (3:1). Metaphase chromosome spreads were prepared on glass microscope slides, stained with Giemsa solution

(Sigma), and counted/analysed using an upright light microscope (Leica DM2500) equipped with a 40x air-lens.

Immunofluorescence and real-time microscopy

For immunofluorescence, MDA-MB-231 cells ($1x10^4$) were seeded in 8-well chamber slides (Lab-Tek, Nunc) and cultured overnight in serum-free medium or CM containing nocodazole (100 ng/ml). The medium was changed to CM and cells were cultured for a further 48 hrs before paraformaldehyde fixation, Triton X-100 permeabilization, and blocking in goat serum containing BSA. Slides were then incubated with primary anti-α-tubulin (Sigma-Aldrich), anti-pericentrin (Abcam), or anti-centrin2 (Santa Cruz) antibodies, followed by species-specific fluorescent secondary antibodies (Molecular Probes). DNA was detected with 1.5 μg/ml 4,6-diamidino-2-phenylindole (VECTASHIELD Mounting Medium with DAPI; Vector Laboratories). Fluorescent images were obtained and processed using an Olympus-Fluoview-FV1000 confocal microscope.

For real-time microscopy, MDA-MB-231 cells co-expressing doxycycline-inducible red fluorescent protein (RFP) and shNek2 were transfected with pBOS human histone 2B-GFP plasmid using Lipofectamine2000 (Invitrogen). Transfected cells ($1x10^4$) were seeded in 8-well chamber slides and cultured overnight as above. The medium was changed to CM with or without doxycycline (500 ng/ml), and cells were cultured and recorded for an additional 150 hrs at 37°C in 5% CO_2. The CM with or without doxycycline was replaced every 48 hrs. Cells were recorded using a Leica DMI 6000B instrument and image analysis was performed using Volocity software.

Immunohistochemistry (IHC)

Tissues were fixed in 10% buffered formalin and embedded in paraffin. Tissue sections (5μm) were stained with hematoxylin and eosin, or subjected to immunohistochemical staining to detect CC-3. Briefly, tissue sections were incubated first with anti-CC-3 antibody (1:250; Cell Signaling), then with biotinylated goat anti-rabbit secondary antibody (1:100, Vector Labs), and exposed to ABC reagent (1:200 final A and B dilution; PK-6100, Vector Labs). The DAB substrate kit (SK-4100, Vector Labs) was used to visualize anti-CC-3 antibody staining. Imaging was performed on a Leica DM2500 microscope.

...The tissue microarray contains 39 triple negative breast cancers from our institution. For each case there were two 0.6 mm biopsy-cores of invasive carcinoma and one of normal breast tissue taken. Invasive carcinoma cells (IDCs) were scored for percentage of cells showing nuclear Nek2 expression. The degree of Nek2 expression intensity was also scored (S=strong, I=intermediate, W=weak). Tissue microarray was microwaved, exposed to Tris-EDTA pH 9.0 and incubated with anti-Nek2 antibody (1:100, BD) over night. The BioGenx polymer kit was used for detection.

Immunoblotting

Cell extracts were prepared in RIPA buffer. Equal amounts of protein were resolved by SDS-PAGE and subjected to standard immunoblotting using antibodies recognizing phospho-Rb, total Rb, phospho-histone H3-Ser10 (all from Cell Signaling); total histone H3 (Abcam); or G6PDH (Sigma).

Statistics

Kaplan-Meier survival plots and intergroup comparison statistics were determined using GraphPad PRISM-5 software. The log-rank test was used to evaluate differences in animal survival among experimental groups (p value). The two-tailed Student's t-test with standard error of the mean (SEM) was used to evaluate differences in all other assays.

Acknowledgements

We thank Dr. Mary Saunders for insightful scientific editing. This work was supported by grant #179815 from the Canadian Institutes of Health Research to TWM. This work was also performed with the support of the Ontario Institute for Cancer Research to PCB through funding provided by the Government of Ontario.

Conflict of interest

The authors declare that no conflicts of interest exist.

Supplementary Information accompanies the paper on the Oncogene website (http://www.nature.com/onc).

References

1. Siegel R, Ward E, Brawley O, Jemal A. Cancer statistics, 2011: the impact of eliminating socioeconomic and racial disparities on premature cancer deaths. CA Cancer J Clin.61(4):212-36.

2. Gennari A, Conte P, Rosso R, Orlandini C, Bruzzi P. Survival of metastatic breast carcinoma patients over a 20-year period: a retrospective analysis based on individual patient data from six consecutive studies. Cancer. 2005;104(8):1742-50.

3. Chia SK, Speers CH, D'Yachkova Y, Kang A, Malfair-Taylor S, Barnett J, et al. The impact of new chemotherapeutic and hormone agents on survival in a population-based cohort of women with metastatic breast cancer. Cancer. 2007;110(5):973-9.

4. Nandini D, Smith BR, Leyland-Jones B. Targeting Basal-Like Breast Cancers. Curr Drug Targets. 2012. Epub 2012/09/15.

5. Reddy KB. Triple-negative breast cancers: an updated review on treatment options. Curr Oncol. 2011;18(4):e173-9. Epub 2011/08/30.

6. Yunokawa M, Koizumi F, Kitamura Y, Katanasaka Y, Okamoto N, Kodaira M, et al. Efficacy of everolimus, a novel mTOR inhibitor, against basal-like triple-negative breast cancer cells. Cancer Sci. 2012;103(9):1665-71. Epub 2012/06/19.

7. Shibata H, Miuma S, Saldivar JC, Huebner K. Response of subtype-specific human breast cancer-derived cells to poly(ADP-ribose) polymerase and checkpoint kinase 1 inhibition. Cancer Sci. 2011;102(10):1882-8. Epub 2011/06/29.

8. Tryfonopoulos D, Walsh S, Collins DM, Flanagan L, Quinn C, Corkery B, et al. Src: a potential target for the treatment of triple-negative breast cancer. Ann Oncol. 2011;22(10):2234-40. Epub 2011/03/02.

9. Loddo M, Kingsbury SR, Rashid M, Proctor I, Holt C, Young J, et al. Cell-cycle-phase progression analysis identifies unique phenotypes of major prognostic and predictive significance in breast cancer. Br J Cancer. 2009;100(6):959-70. Epub 2009/02/26.

10. Hu K, Law JH, Fotovati A, Dunn SE. Small interfering RNA library screen identified polo-like kinase-1 (PLK1) as a potential therapeutic target for breast cancer that uniquely eliminates tumor-initiating cells. Breast Cancer Res. 2012;14(1):R22. Epub 2012/02/09.

11. Romanelli A, Clark A, Assayag F, Chateau-Joubert S, Poupon MF, Servely JL, et al. Inhibiting Aurora kinases reduces tumor growth and suppresses tumor recurrence after chemotherapy in patient-derived triple-negative breast cancer xenografts. Mol Cancer Ther. 2012. Epub 2012/09/27.

12. Fiskus W, Hembruff SL, Rao R, Sharma P, Balusu R, Venkannagari S, et al. Co-treatment with vorinostat synergistically enhances activity of Aurora kinase inhibitor against human breast cancer cells. Breast Cancer Res Treat. 2012;135(2):433-44. Epub 2012/07/25.

13. Arpaia E, Blaser H, Quintela-Fandino M, Duncan G, Leong HS, Ablack A, et al. The interaction between caveolin-1 and Rho-GTPases promotes metastasis by controlling the expression of alpha5-integrin and the activation of Src, Ras and Erk. Oncogene. 2012;31(7):884-96. Epub 2011/07/19.

14. Fry AM, Schultz SJ, Bartek J, Nigg EA. Substrate specificity and cell cycle regulation of the Nek2 protein kinase, a potential human homolog of the mitotic regulator NIMA of Aspergillus nidulans. J Biol Chem. 1995;270(21):12899-905.

15. Fry AM, O'Regan L, Sabir SR, Bayliss R. Cell cycle regulation by the NEK family of protein kinases. J Cell Sci. 2012;125(Pt 19):4423-33. Epub 2012/11/08.

16. Fry AM, Meraldi P, Nigg EA. A centrosomal function for the human Nek2 protein kinase, a member of the NIMA family of cell cycle regulators. EMBO J. 1998;17(2):470-81. Epub 1998/02/28.

17. Ha Kim Y, Yeol Choi J, Jeong Y, Wolgemuth DJ, Rhee K. Nek2 localizes to multiple sites in mitotic cells, suggesting its involvement in multiple cellular functions during the cell cycle. Biochem Biophys Res Commun. 2002;290(2):730-6. Epub 2002/01/12.

18. Fry AM. The Nek2 protein kinase: a novel regulator of centrosome structure. Oncogene. 2002;21(40):6184-94.

19. Hayward DG, Clarke RB, Faragher AJ, Pillai MR, Hagan IM, Fry AM. The centrosomal kinase Nek2 displays elevated levels of protein expression in human breast cancer. Cancer Res. 2004;64(20):7370-6.

20. Richardson AL, Wang ZC, De Nicolo A, Lu X, Brown M, Miron A, et al. X chromosomal abnormalities in basal-like human breast cancer. Cancer cell. 2006;9(2):121-32. Epub 2006/02/14.

21. Komatsu M, Yoshimaru T, Matsuo T, Kiyotani K, Miyoshi Y, Tanahashi T, et al. Molecular features of triple negative breast cancer cells by genome-wide gene expression profiling analysis. International journal of oncology. 2013;42(2):478-506. Epub 2012/12/21.

22. Gyorffy B, Lanczky A, Eklund AC, Denkert C, Budczies J, Li Q, et al. An online survival analysis tool to rapidly assess the effect of 22,277 genes on breast cancer prognosis using microarray data of 1,809 patients. Breast Cancer Res Treat. 2010;123(3):725-31. Epub 2009/12/19.

23. Tsunoda N, Kokuryo T, Oda K, Senga T, Yokoyama Y, Nagino M, et al. Nek2 as a novel molecular target for the treatment of breast carcinoma. Cancer Sci. 2009;100(1):111-6.

24. Mittnacht S. Control of pRB phosphorylation. Curr Opin Genet Dev. 1998;8(1):21-7. Epub 1998/04/08.

25. Hans F, Dimitrov S. Histone H3 phosphorylation and cell division. Oncogene. 2001;20(24):3021-7. Epub 2001/06/23.

26. Hayward DG, Fry AM. Nek2 kinase in chromosome instability and cancer. Cancer Lett. 2006;237(2):155-66. Epub 2005/08/09.

27. Kokuryo T, Senga T, Yokoyama Y, Nagino M, Nimura Y, Hamaguchi M. Nek2 as an effective target for inhibition of tumorigenic growth and peritoneal dissemination of cholangiocarcinoma. Cancer Res. 2007;67(20):9637-42. Epub 2007/10/19.

28. O'Regan L, Blot J, Fry AM. Mitotic regulation by NIMA-related kinases. Cell Div. 2007;2:25. Epub 2007/08/31.

29. Mardin BR, Schiebel E. Breaking the ties that bind: new advances in centrosome biology. The Journal of cell biology. 2012;197(1):11-8. Epub 2012/04/05.

30. Chen Y, Riley DJ, Zheng L, Chen PL, Lee WH. Phosphorylation of the mitotic regulator protein Hec1 by Nek2 kinase is essential for faithful chromosome segregation. J Biol Chem. 2002;277(51):49408-16. Epub 2002/10/19.

31. Lou Y, Yao J, Zereshki A, Dou Z, Ahmed K, Wang H, et al. NEK2A interacts with MAD1 and possibly functions as a novel integrator of the spindle checkpoint signaling. J Biol Chem. 2004;279(19):20049-57. Epub 2004/02/24.

32. Carter SL, Eklund AC, Kohane IS, Harris LN, Szallasi Z. A signature of chromosomal instability inferred from gene expression profiles predicts clinical outcome in multiple human cancers. Nat Genet. 2006;38(9):1043-8. Epub 2006/08/22.

33. Kolodner RD, Cleveland DW, Putnam CD. Cancer. Aneuploidy drives a mutator phenotype in cancer. Science. 2011;333(6045):942-3. Epub 2011/08/20.

34. Liu Q, Hirohashi Y, Du X, Greene MI, Wang Q. Nek2 targets the mitotic checkpoint proteins Mad2 and Cdc20: a mechanism for aneuploidy in cancer. Exp Mol Pathol.88(2):225-33.

35. De Souza CP, Osmani AH, Wu LP, Spotts JL, Osmani SA. Mitotic histone H3 phosphorylation by the NIMA kinase in Aspergillus nidulans. Cell. 2000;102(3):293-302. Epub 2000/09/07.

36. Di Agostino S, Rossi P, Geremia R, Sette C. The MAPK pathway triggers activation of Nek2 during chromosome condensation in mouse spermatocytes. Development. 2002;129(7):1715-27. Epub 2002/03/30.

37. Du J, Cai X, Yao J, Ding X, Wu Q, Pei S, et al. The mitotic checkpoint kinase NEK2A regulates kinetochore microtubule attachment stability. Oncogene. 2008;27(29):4107-14. Epub 2008/02/26.

38. Ferretti C, Totta P, Fiore M, Mattiuzzo M, Schillaci T, Ricordy R, et al. Expression of the kinetochore protein Hec1 during the cell cycle in normal and cancer cells and its regulation by the pRb pathway. Cell Cycle. 2010;9(20):4174-82. Epub 2010/10/16.

39. Ikui AE, Yang CP, Matsumoto T, Horwitz SB. Low concentrations of taxol cause mitotic delay followed by premature dissociation of p55CDC from Mad2 and BubR1 and abrogation of the spindle checkpoint, leading to aneuploidy. Cell Cycle. 2005;4(10):1385-8. Epub 2005/09/03.

40. Hayward DG, Newbatt Y, Pickard L, Byrne E, Mao G, Burns S, et al. Identification by high-throughput screening of viridin analogs as biochemical and cell-based inhibitors of the cell cycle-regulated nek2 kinase. J Biomol Screen. 2010;15(8):918-27. Epub 2010/07/29.

41. Shaukat Z, Wong HW, Nicolson S, Saint RB, Gregory SL. A screen for selective killing of cells with chromosomal instability induced by a spindle checkpoint defect. PloS one. 2012;7(10):e47447. Epub 2012/10/19.

42. Zhou W, Yang Y, Xia J, Wang H, Salama ME, Xiong W, et al. NEK2 induces drug resistance mainly through activation of efflux drug pumps and is associated with poor prognosis in myeloma and other cancers. Cancer cell. 2013;23(1):48-62. Epub 2013/01/19.

43. Wang S, Li W, Liu N, Zhang F, Liu H, Liu F, et al. Nek2A contributes to tumorigenic growth and possibly functions as potential therapeutic target for human breast cancer. J Cell Biochem. 2012;113(6):1904-14. Epub 2012/01/12.

44. Innocenti P, Cheung KM, Solanki S, Mas-Droux C, Rowan F, Yeoh S, et al. Design of potent and selective hybrid inhibitors of the mitotic kinase Nek2: structure-activity relationship, structural biology, and cellular activity. Journal of medicinal chemistry. 2012;55(7):3228-41. Epub 2012/03/13.

45. Lee J, Gollahon L. Nek2-targeted ASO or siRNA pretreatment enhances anticancer drug sensitivity in triple negative breast cancer cells. International journal of oncology. 2013;42(3):839-47. Epub 2013/01/24.

Figure 1

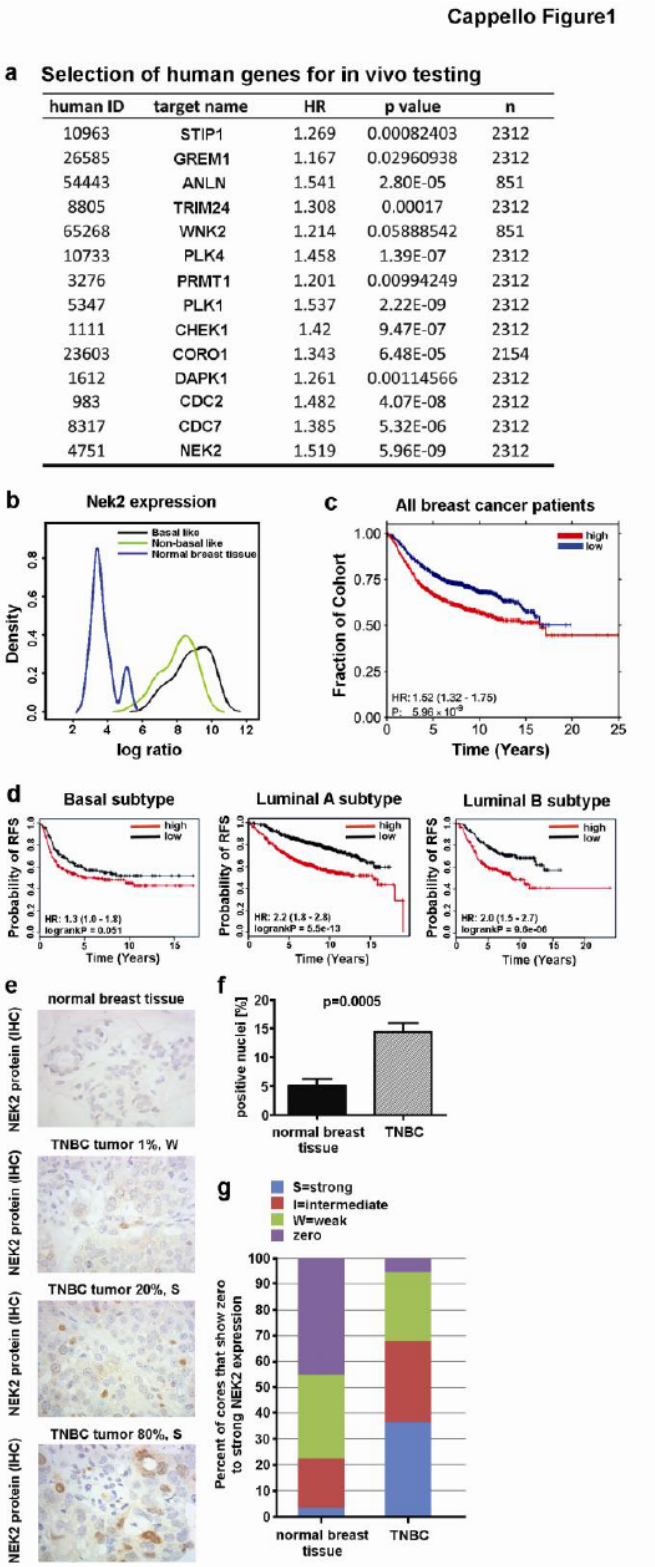

human ID	target name	HR	p value	n
10963	STIP1	1.269	0.00082403	2312
26585	GREM1	1.167	0.02960938	2312
54443	ANLN	1.541	2.80E-05	851
8805	TRIM24	1.308	0.00017	2312
65268	WNK2	1.214	0.05888542	851
10733	PLK4	1.458	1.39E-07	2312
3276	PRMT1	1.201	0.00994249	2312
5347	PLK1	1.537	2.22E-09	2312
1111	CHEK1	1.42	9.47E-07	2312
23603	CORO1	1.343	6.48E-05	2154
1612	DAPK1	1.261	0.00114566	2312
983	CDC2	1.482	4.07E-08	2312
8317	CDC7	1.385	5.32E-06	2312
4751	NEK2	1.519	5.96E-09	2312

Figure 2

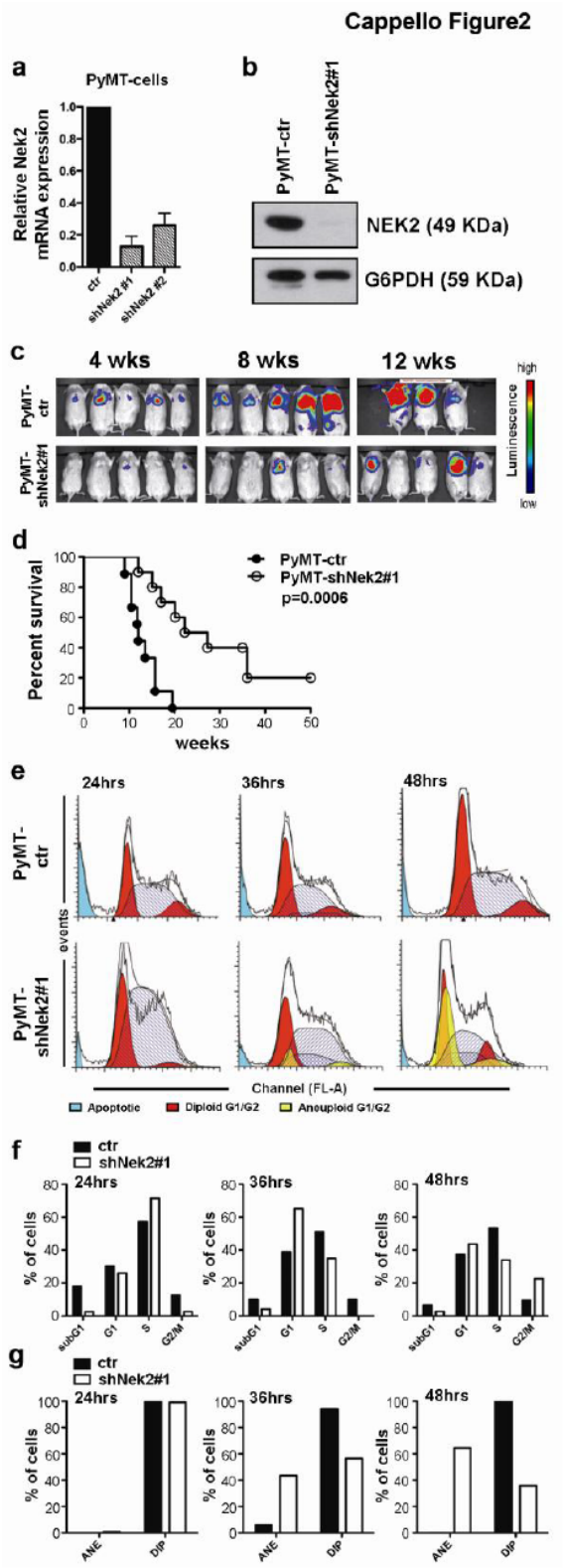
Cappello Figure2
a
PyMT-cells
Relative Nek2 mRNA expression
ctr
shNek2 #1
shNek2 #2
b
PyMT-ctr
PyMT-shNek2#1
NEK2 (49 KDa)
G6PDH (59 KDa)
c
4 wks
8 wks
12 wks
PyMT-ctr
PyMT-shNek2#1
high
Luminescence
low
d
Percent survival
weeks
PyMT-ctr
PyMT-shNek2#1
p=0.0006
e
24hrs
36hrs
48hrs
PyMT-ctr
PyMT-shNek2#1
events
Channel (FL-A)
Apoptotic
Diploid G1/G2
Aneuploid G1/G2
f
ctr
shNek2#1
24hrs
36hrs
48hrs
% of cells
subG1
G1
S
G2/M
g
ctr
shNek2#1
24hrs
36hrs
48hrs
% of cells
ANE
DIP

Figure 3

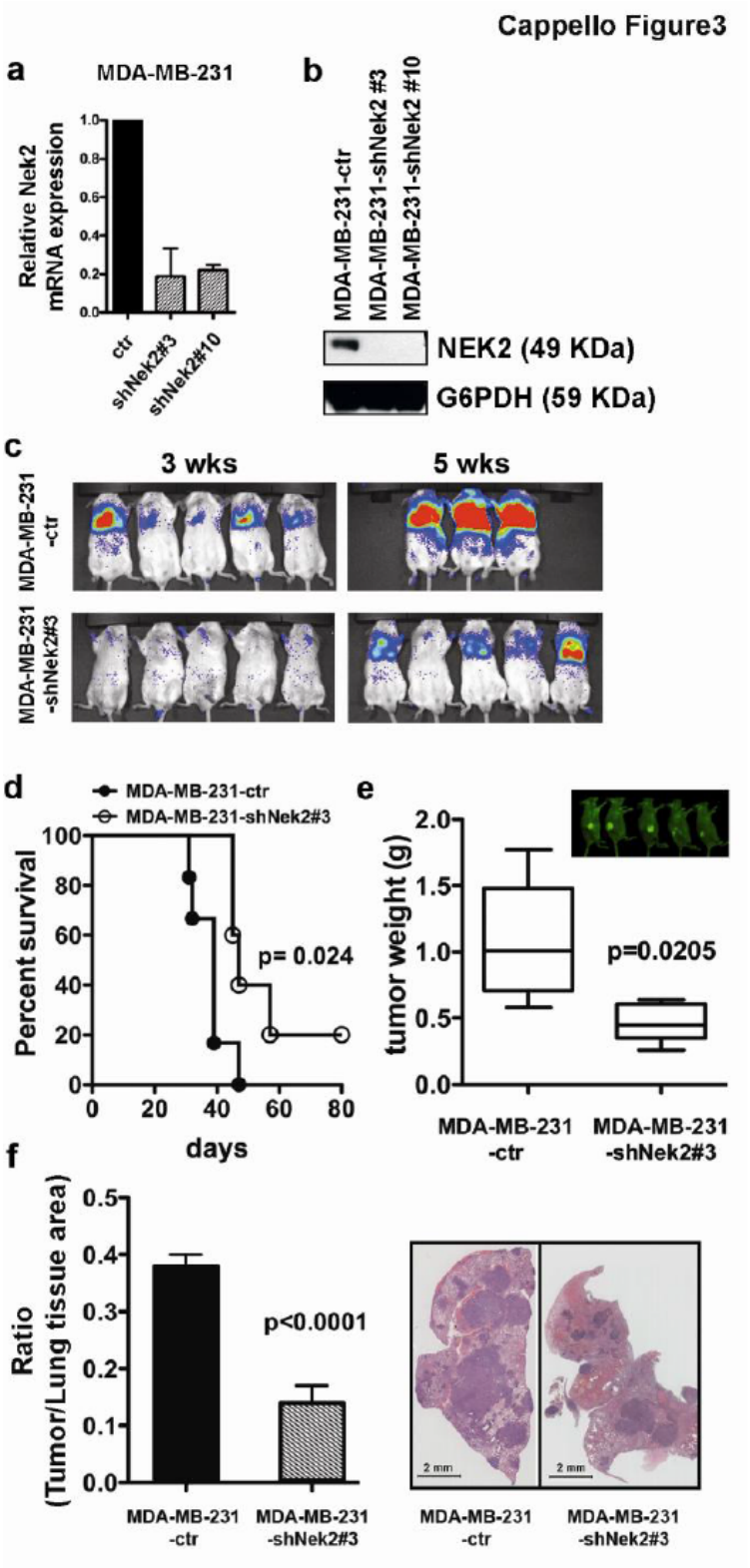
Cappello Figure3
a
MDA-MB-231
Relative Nek2 mRNA expression
1.0
0.8
0.6
0.4
0.2
0.0
ctr
shNek2#3
shNek2#10
b
MDA-MB-231-ctr
MDA-MB-231-shNek2 #3
MDA-MB-231-shNek2 #10
NEK2 (49 KDa)
G6PDH (59 KDa)
c
3 wks
5 wks
MDA-MB-231 -ctr
MDA-MB-231 -shNek2#3
d
MDA-MB-231-ctr
MDA-MB-231-shNek2#3
Percent survival
100
80
60
40
20
0
0
20
40
60
80
days
p= 0.024
e
tumor weight (g)
2.0
1.5
1.0
0.5
0.0
p=0.0205
MDA-MB-231 -ctr
MDA-MB-231 -shNek2#3
f
Ratio (Tumor/Lung tissue area)
0.5
0.4
0.3
0.2
0.1
0.0
p<0.0001
MDA-MB-231 -ctr
MDA-MB-231 -shNek2#3
2 mm
2 mm
MDA-MB-231 -ctr
MDA-MB-231 -shNek2#3

Figure 4

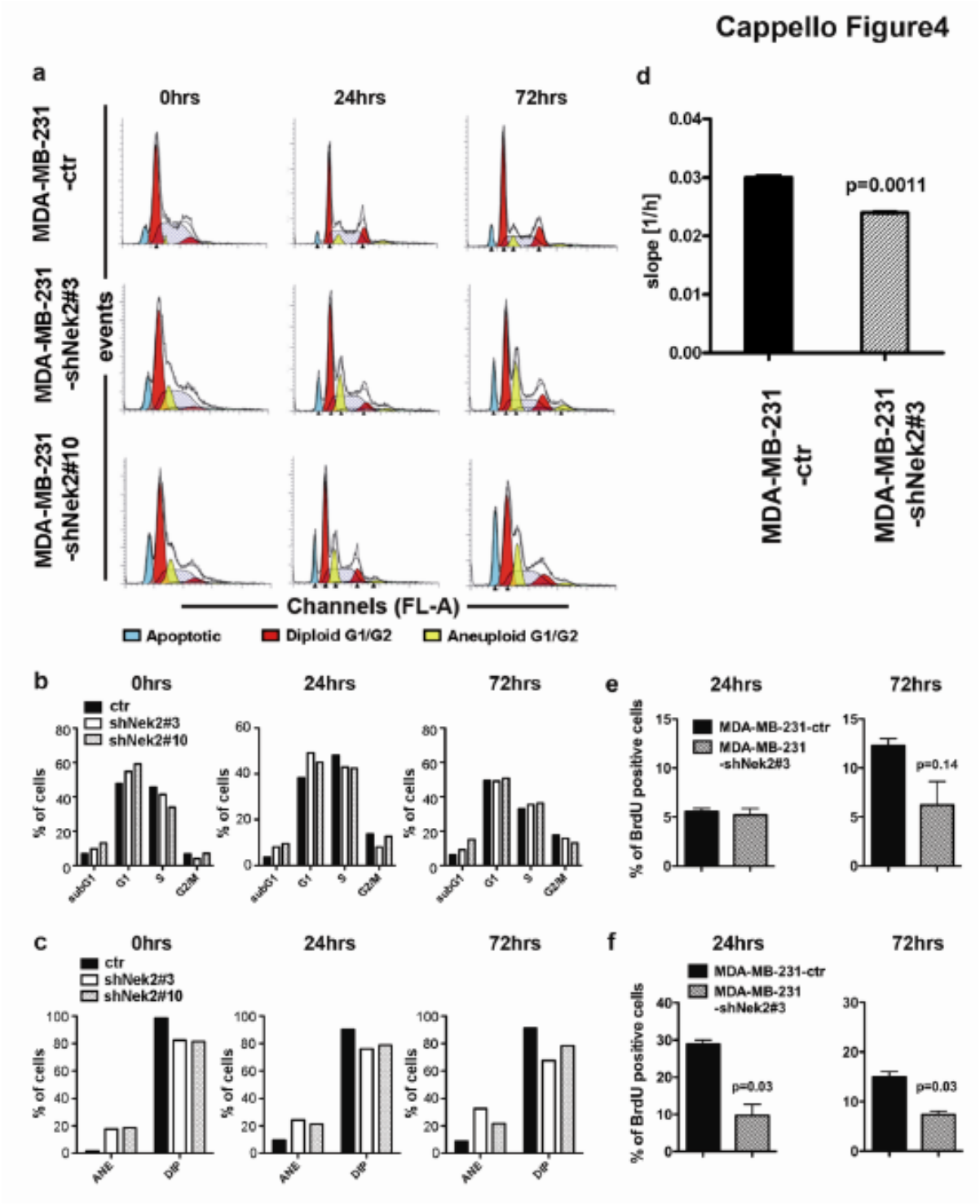
Cappello Figure4
a
0hrs
24hrs
72hrs
MDA-MB-231 -ctr
MDA-MB-231 -shNek2#3
MDA-MB-231 -shNek2#10
events
Channels (FL-A)
Apoptotic
Diploid G1/G2
Aneuploid G1/G2
d
slope [1/h]
p=0.0011
MDA-MB-231 -ctr
MDA-MB-231 -shNek2#3
b
ctr
shNek2#3
shNek2#10
% of cells
subG1
G1
S
G2/M
e
MDA-MB-231-ctr
MDA-MB-231 -shNek2#3
% of BrdU positive cells
p=0.14
c
ANE
DIP
f
p=0.03

Figure 5

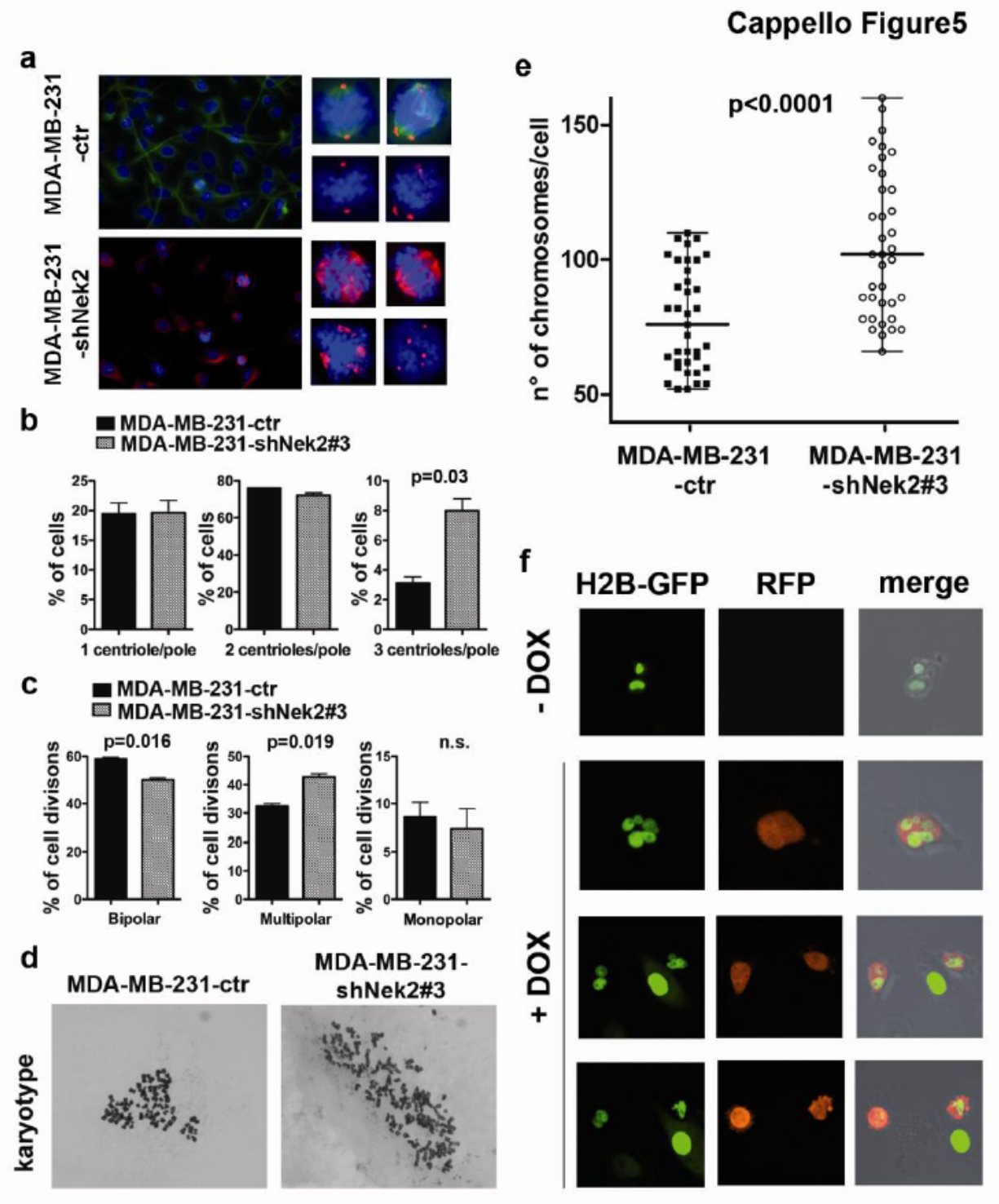
Cappello Figure5
a
MDA-MB-231 -ctr
MDA-MB-231 -shNek2
b
MDA-MB-231-ctr
MDA-MB-231-shNek2#3
% of cells
1 centriole/pole
2 centrioles/pole
3 centrioles/pole
p=0.03
c
MDA-MB-231-ctr
MDA-MB-231-shNek2#3
% of cell divisons
p=0.016
p=0.019
n.s.
Bipolar
Multipolar
Monopolar
d
MDA-MB-231-ctr
MDA-MB-231-shNek2#3
karyotype
e
p<0.0001
n° of chromosomes/cell
MDA-MB-231 -ctr
MDA-MB-231 -shNek2#3
f
H2B-GFP
RFP
merge
- DOX
+ DOX

Figure 6

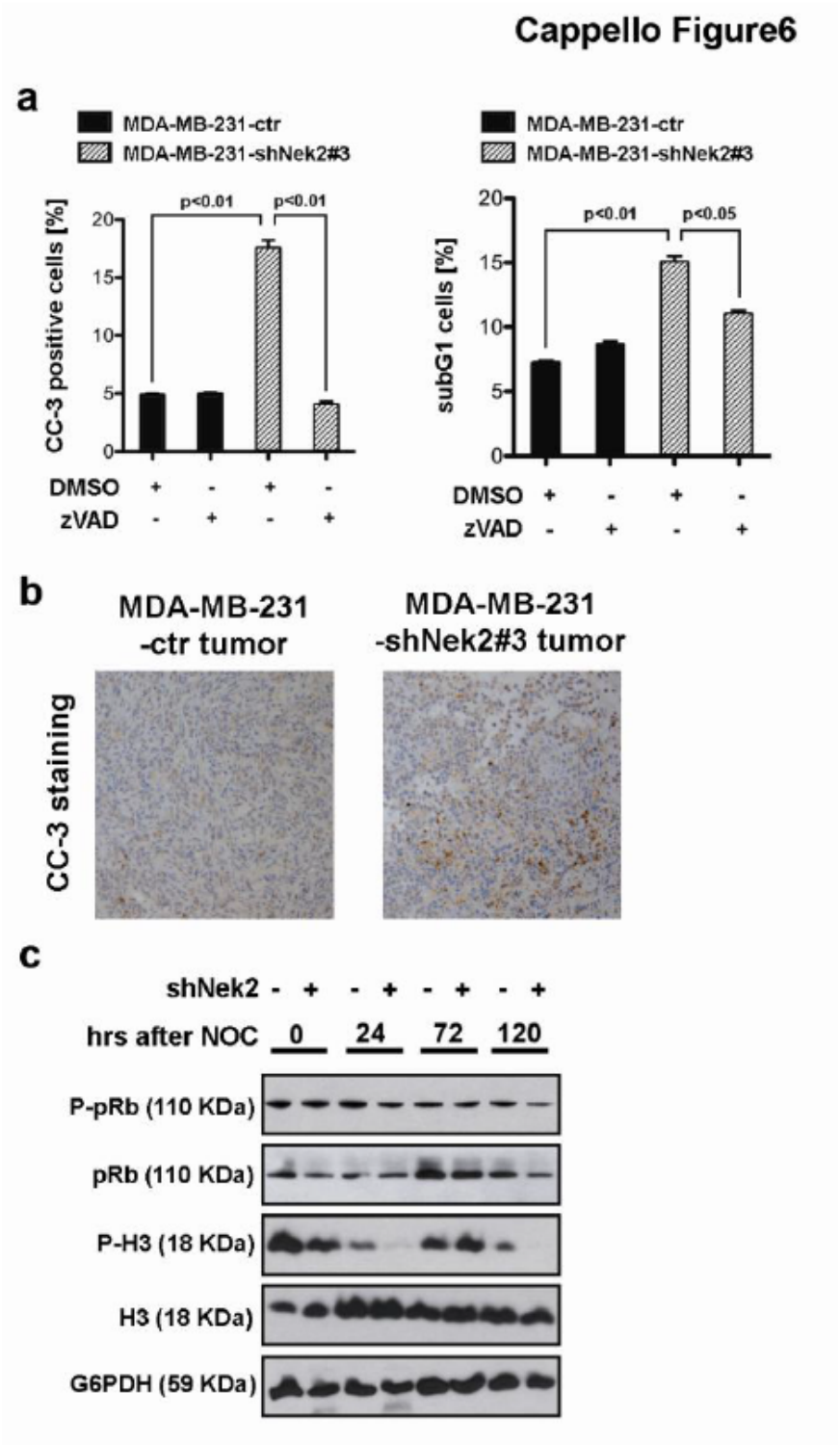
Cappello Figure6
a
MDA-MB-231-ctr
MDA-MB-231-shNek2#3
CC-3 positive cells [%]
p<0.01
p<0.01
DMSO
zVAD
subG1 cells [%]
p<0.01
p<0.05
b
MDA-MB-231 -ctr tumor
MDA-MB-231 -shNek2#3 tumor
CC-3 staining
c
shNek2
hrs after NOC
0
24
72
120
P-pRb (110 KDa)
pRb (110 KDa)
P-H3 (18 KDa)
H3 (18 KDa)
G6PDH (59 KDa)

Figure Legends

Figure 1. Target selection for *in vivo* tumor growth study and characterization of Nek2 in human breast cancers.

(a) Selected human genes associated with poor breast cancer patient prognosis. The human gene ID number and target name are indicated, as well as each target's hazard ratio (HR) related to overall patient survival, the p value, and the number (n) of breast cancer patients analyzed for that target. (b) Relative Nek2 mRNA expression (density) in normal breast tissue, basal-like or non-basal-like breast cancer tissues, extrapolated from the Richardson data set (20). (c) Survival curve for a cohort of 2312 breast cancer patients stratified based on high or low Nek2 expression in the patient's tumor. The HR and p values for the correlation between Nek2 level and patient prognosis are indicated. (d) Relapse-free survival curves (RFS) of patients bearing breast cancers of the basal, luminal A or luminal B subtypes, stratified based on high or low Nek2 expression in the patient's tumor (22). The HR and p values for the correlation between Nek2 level and patient prognosis are indicated. (e) IHC, NEK2 protein expression in triple-negative breast cancers (TNBC) from a cohort of 39 patients. 3 representative examples of NEK2 expression in TNBCs (1% positive nuclei – W=weak intensity; 20% positive nuclei – S=strong intensity; 80% positive nuclei – S=strong intensity) are shown in comparison to normal breast tissue (zero intensity). (f) NEK2 positive nuclei per biopsy-core. Mean percentage ± SEM. (g) Percentage of biopsy-cores (total 39 TNBCs and 39 corresponding controls of normal breast tissue, see Supplementary Table S1) that show S=strong, I=intermediate, W=weak and zero staining intensity.

Figure 2. Nek2 promotes mouse tumor cell growth *in vivo*.

(a) qRT-PCR analysis of Nek2 mRNA expression in mouse PyMT cells transduced with lentiviral vectors expressing control scramble shRNA (ctr) or shNek2 #1 or #2. Data were normalized to Gapdh mRNA and expressed relative to levels in control cells (set to 1.0). Results are the mean ± SEM of triplicates. (b) Immunoblot of Nek2 protein in the PyMT-ctr and PyMT-shNek2 cells in (a). G6PDH, loading control. (c) Time course of the *in vivo* growth of PyMT-ctr and PyMT-shNek2 cells injected into the tail veins of female 129P2Ola mice. Mice were subjected to whole animal imaging using an IVIS Spectrum Imaging system at the indicated timepoints post-injection. Scaling intensity of images was normalized to control. One group of 5 animals per experimental condition is shown. (d) Kaplan-Meier survival curve of the mice in (c) (n=5/group). (e) Flow cytometric cell cycle analysis of serum-starved PyMT-ctr and PyMT-shNek2 cells at the indicated timepoints after serum replenishment. Red peaks, G1 and G2/M phases of diploid cells; blue peak, subG1 phase (dead cells); yellow peaks, G1 and G2/M phases of aneuploid cells. Results are representative of three independent experiments. (f) Quantitation of the cell cycle analyses in (e). (g) Quantitation of the percentages of the cells in (e) that were diploid (DIP) or aneuploid (ANE). For (e), (f) and (g), representative results are shown out of triplicates.

Figure 3. Lack of Nek2 reduces the growth of MDA-MB-231 cells *in vivo*.

(a) qRT-PCR analysis of Nek2 mRNA expression in human MDA-MB-231 cells transduced with lentiviral vectors expressing control scramble shRNA (ctr) or shNek2 #3 or #10. Data were analyzed relative to GAPDH mRNA levels as in Figure 2a. Results are the mean ± SEM of triplicates. (b) Immunoblot of Nek2 protein in the MDA-MB-231-ctr and MDA-MB-231-shNek2 #3 or #10 cells in (a) analyzed as in Figure 2b. (c) Time course of the *in vivo* growth of MDA-

MB-231-ctr and MDA-MB-231-shNek2#3 cells injected into the tail veins of NOD-SCID mice. Mice were subjected to whole animal imaging and analyzed as in Figure 2c. (d) Kaplan-Meier survival curve of the mice in (c). (e) Weights of tumors excised from NIH-III nu/nu mice whose fat pads were injected with MDA-MB-231-ctr or MDA-MB-231-shNek2#3 cells. Data are the mean of 5 tumors per group ± SEM. Inset: GFP-positive MDA-MB-231-shNek2#3 cells are clearly evident in the fat pads of all injected mice, confirming the expression of the shNek2 lentiviral vector. (f) Left panel: Quantitation of the ratio of 'tumor tissue area/lung tissue area' in mice IV-injected with MDA-MB-231-ctr or MDA-MB-231-shNek2#3 cells at 35 days post-injection. Data are the mean of 3 sections per 2 lungs per group ± SEM. Right panel: Representative H&E-stained sections of lungs from the IV-injected mice in the left panel.

Figure 4. Nek2 knockdown induces cell growth arrest, aneuploidy and aberrant mitosis.
(a) Flow cytometric cell cycle analysis of MDA-MB-231-ctr and MDA-MB-231-shNek2 #3 and #10 cells at the indicated timepoints after serum starvation. Data were analyzed as in Figure 2e. (b) Quantitation of the cell cycle analyses in (a). (c) Quantitation of percentages of the cells in (a) that were diploid (DIP) or aneuploid (ANE). (d) Evaluation of the real-time proliferation of MDA-MB-231-ctr and MDA-MB-231-shNek2#3 cells using an xCELLigence RTCA DP instrument. Data are expressed as the slope [1/h], where a higher slope represents faster cell growth. (e) Quantitation of the percentage of $BrdU^+$ cells (replicating cells) of MDA-MB-231-ctr and MDA-MB-231-shNek2#3 cultures at the indicated times after serum starvation. (f) Quantitation of the percentage of $BrdU^+$ cells in MDA-MB-231-ctr and MDA-MB-231-shNek2#3 cultures at the indicated times after nocodazole treatment. For (a), (b) and (c) results

are representative of three independent experiments. For (d), (e) and (f), results are the mean ± SEM of triplicates.

Figure 5. Nek2 knockdown increases centriole numbers, causes multinucleation, and aneuploidy.

(a) Immunofluorescent analysis of centrosomes (red) and microtubules (green in MDA-MB-231-ctr cells, and red in GFP-expressing MDA-MB-231-shNek2 cells) in dividing control and Nek2 knockdown cells at 48 hrs after nocodazole treatment. Smaller panels on the right are higher magnification images of representative cells in the left panels. Results are representative of two independent experiments. (b) Quantitation of the numbers of centrioles per pole in the MDA-MB-231-ctr and MDA-MB-231-shNek2#3 in (a) (n=60/group) determined by staining with anti-centrin2 antibody. (c) Quantitation of the bipolar, multipolar and monopolar divisions of the cells in (a) (n=60 cells/group) determined by staining with anti-α-tubulin antibody. (d) Metaphase chromosome spreads of MDA-MB-231-ctr and MDA-MB-231-shNek2 cells vizualized by Giemsa staining. Images are representative of 35 cells/group examined. (e) Quantitation of total chromosome numbers in the MDA-MB-231-ctr and MDA-MB-231-shNek2 cells in (d). (f) Snapshots from real-time microscopy generating Supplementary Movies 1 and 2. The mitosis of MDA-MB-231 cells expressing doxycycline (DOX)-inducible shNek2 and RFP (red), along with H2B-GFP (green), was followed. Multinucleated cells can be seen in images of DOX-treated (Nek2 knockdown) cells. The "Merge" column contains overlaid images of the red, green and bright fields. For (b), (c) and (e), results are the mean ± SEM.

Figure 6. Nek2 knockdown increases cleaved caspase-3 and alters pRB and histone H3 phosphorylation.

(a) Quantitation of CC-3$^+$ cells and subG1 cells (dead cells) in cultures of MDA-MB-231-ctr and MDA-MB-231-shNek2#3 cells that were serum-starved overnight and cultured for 48 hrs in CM plus DMSO alone (vehicle) or DMSO containing zVAD, as indicated. Percentages of CC-3$^+$ (left) and subG1 (right) cells were determined by flow cytometry. Data are the mean ± SEM and are representative of two independent experiments. (b) Immunohistochemical analysis of CC-3$^+$ cells in tumors of NIH-III mice whose fat pads were injected with MDA-MB-231-ctr or MDA-MB-231-shNek2#3 cells. Results are representative of 5 tumors/group examined. (c) Immunoblot to detect the indicated proteins in extracts of MDA-MB-231-ctr (-) and MDA-MB-231-shNek2#3 (+) cells at the indicated timepoints after release from nocodazole (NOC) treatment. G6PDH, loading control.